Desalination and Water Treatment
www.deswater.com

doi:10.5004/dwt.2020.24974

178 (2020) 211–219
February

Possibility of using granular iron slag by-product as permeable reactive barrier for remediation of simulated water contaminated with lead ions

Saif S. Alquzweeni[a], Ayad A.H. Faisal[b,*]

[a]*Department of Civil Engineering, College of Engineering, University of Babylon, Babylon, Iraq, email: saifalquzweeni@gmail.com*
[b]*Department of Environmental Engineering, College of Engineering, University of Baghdad, Baghdad, Iraq, Tel. +964 7904208688; email: ayadabedalhamzafaisal@yahoo.com*

Received 13 June 2019; Accepted 25 September 2019

ABSTRACT

For the application of sustainability concepts, this study investigates the possibility of using iron slag by-product as reactive material in the permeable reactive barrier technology. This investigation was achieved based on the set of batch equilibrium and kinetic tests in combination with the prediction of the barrier – retardation factor as the main indicator for the longevity of this barrier. Results reveal that the removal efficiency was greater than 90% at best operational conditions specified by changing the pH, contact time, sorbent dosage, and agitation speed in the ranges of 3–7, 0–180 min, 0.5–12 g/100 mL, 0–250 rpm respectively for lead ions initial concentration of 50 mg/L. The maximum adsorption capacity of iron slag can be calculated by the Langmuir model because it is more representative of sorption data. This capacity (=2.309 mg/g) is compatible with the value calculated from pseudo-second-order which describes the kinetic data in a good manner, so, the ion exchange or chemisorption can be the predominant mechanism for sorption of lead ions. The X-ray diffraction, Fourier transform infrared spectroscopy, scanning electron microscopy and energy-dispersive X-ray spectroscopy tests for reactive material supported this result where the dissolution of calcium oxide by hydrolysis and ion exchange can enhance the removal of lead ions by iron oxide surface sites.

Keywords: Iron slag; Permeable barrier; Isotherm; Kinetic; Retardation factor

1. Introduction

Water supply systems and ecosystem health can be suffered from a serious threat due to contamination of groundwater with heavy metals such as lead ions [1]; therefore, the remediation of groundwater must be adopted to avoid this threat. Permeable reactive barriers (PRBs) are passive remediation technology that applied within the site to restore the contaminated groundwater using certain material. The availability, cost-effective, permeability, reactivity, and long-term stability are the main characteristics of the materials used in the PRB. This technique is considered an efficient alternative for conventional methods such as pump and treat system in the remediation of the contaminated groundwater. Accordingly, the choice of reactive material that can be used in the PRB is considered a critical point in specifying the performance and longevity of the barrier [2–5].

Although the activated carbon, zeolite and other conventional sorbents have a good ability in the removal of a wide broad of the inorganic contaminants, the high cost of these materials was the cause for their limiting usage [6–8]. Hence, finding the non-conventional low-cost materials with good ability in the reduction of pollution opens new horizons for many studies. By-products resulted from different industries such as fly ash, bottom ash, and iron slag as well as agricultural wastes such as rice husk and tree bark can be tested

* Corresponding author.

to find their suitability for the PRB. In this direction, many previous studies are implemented using waste foundry sand [9,10], cement kiln dust [11], granular dead anaerobic sludge [12,13], zero-valent iron [14], raw scrap iron-aluminum waste [15] and olive pips [16] as sorbent within the PRB.

Iron slag is the main component resulted from a by-product from the steel-making process, however, reuse of this waste has received great attention because of its useful properties [17]. Metal oxides such as calcium oxide, magnesium oxide, and others represent the major constituents of the slag and this composition is similar to Portland cement; however, the slag can be used as filler in the road construction [18–20]. For the sorption properties of slag, several studies were conducted to use this material for the removal of heavy metals from wastewaters [21,22]. Batch tests for the interaction of copper ions with iron slag were implemented for specifying the mechanisms responsible for the removal process under the influence of pH for aqueous solution [23]. Under different operational conditions, the sorption of nickel from contaminated water using converter slag produced from the steel industry is mainly achieved by magnetite. The results proved that the adsorption rate can be increased due to the increase of the initial metal concentration and reduced with the increase of temperature. Also, the Freundlich isotherm model has a good ability in the representation of the measured sorption data [22]. Industrial wastewater contaminated with lead were treated using a set of column packed with electric arc furnace slag/granular blast furnace slag. Results signified that the velocity of the flow and metal concentration have potential effects on the removal of the lead ions within the used columns [24].

Based on the type of the pollutant (i.e. organic or inorganic compounds), the dissolved plume of the contaminant can be created within the aquifer when the spillage of these compounds occurred. There are three main mechanisms will govern the transport of this plume namely; the advection, hydrodynamic dispersion, and reaction where they can be expressed mathematically by "Advection–Dispersion–Reaction equation". The reaction term can be caused a decrease in the concentration of the transported contaminant when the sorption is the predominant mechanism within the reactive medium. Finding the governed isotherm model for the representation of this process will play a vital role in the description of the migration of contaminants within the PRB. Accordingly, the most important point of the present study is finding the reaction (i.e. sorption) term in the solute transport equation by using a suitable isotherm model due to the interaction of lead and iron slag based on batch tests. Consequently, the possibility of using an iron slag by-product in the treatment of simulated water contaminated with lead ions under different operational conditions and finding the mechanisms governed the removal process can be achieved.

2. Description of sorption data

The sorption isotherms describe the relationship between adsorption capacity (q_e) and the remaining concentration of metal in the bulk solution (C_e) [25]. Freundlich and Langmuir models [26] described below can be used to represent this relationship at constant temperature and pH:

Freundlich model (1906): is the earliest known sorption isotherm equation and can be written as follows:

$$q_e = K_F C_e^{\frac{1}{n}} \tag{1}$$

where K_F is a constant related to the maximum adsorption capacity of the sorbent and n is represented the intensity of sorption.

Langmuir model (1916): can be written as follows:

$$q_e = \frac{q_{\max} b C_e}{1 + b C_e} \tag{2}$$

where $q_{\max}$ is the maximum adsorption capacity (mg/g) and b is the dissociation coefficient of the solute–adsorbent complex. The b represents the affinity between the solute and the adsorbent-meaning that a higher b value corresponds to a higher affinity [27].

In addition, the kinetic models (Eqs. (3)–(5)) are applied to find the rate at which the pollutants removed from contaminated water and they can be used for designing the sorption process [28–30].

Pseudo-first-order:

$$q_t = q_e\left[1 - \exp\left(-k_1 t\right)\right] \tag{3}$$

Pseudo-second-order:

$$q_t = \frac{k_2 q_e^2 t}{\left(1 + k_2 q_e t\right)} \tag{4}$$

Intra-particle diffusion equation:

$$q_t = k_{\text{int}} t^{0.5} + C \tag{5}$$

The initial adsorption rate (h) can be determined from k_2 and q_e values using the following equation:

$$h = k_2 q_e^2 \tag{6}$$

where k_1 is the equilibrium rate constant of pseudo-first-order sorption (1/min), k_2 is the rate constant of sorption (g/mg min), k_{int} is the adsorption rate constant of the intra-particle diffusion model (mg/g $\text{min}^{0.5}$), C is the value of intercept which gives an idea about the boundary layer thickness, q_e is the adsorption capacity at equilibrium (mg/g), and q_t is the adsorption capacity at time t (mg/g).

3. Materials and methods

3.1. Sorbent and contaminant

Iron slag by-product was collected from steel and iron factory in Al-Talee'a city, Babylon Governorate, Iraq. It is washed with distilled water to remove fine powder and, then, dried at 383 K for 24 h. Based on the sieve analysis, the particle size distribution was ranged from 0.6 to 1 mm with a geometric mean diameter of 0.775 mm. The hydraulic

conductivity, bulk density, porosity, and Brunauer–Emmett–Teller surface area of this material have the values of 2.69×10^{-3} m/s, 2.026 g/cm^3, 0.41, and 0.2571 m^2/g, respectively. The chemical composition of iron slag was determined by X-ray fluorescence spectroscopy (XRF) analysis using (XRF Spectro-Germany). In addition, the mineralogical composition of iron slag was performed at room temperature (25°C) using X-ray diffraction (XRD).

The lead was selected to represent the heavy metal and a standard solution of this metal with a concentration of 1,000 mg/L can be prepared by dissolving 1.5985 g of $Pb(NO_3)_2$ in 1 L of distilled water. The prepared solution was kept at room temperature and the pH was adjusted by adding 0.1 M HNO_3 or 0.1 M NaOH as required.

3.2. Batch experiments

Batch experiments were conducted to obtain the equilibrium data and to specify the best conditions for the treatment process. The conditions include the contact time, initial pH, granular iron slag dosage, initial concentration of metal, and agitation speed. A number of 250 mL conical-flasks can be used and 100 mL of metal solution with an initial concentration of 50 mg/L was put in each flask. A certain quantity of iron slag (3.0 g) was added to each flask and the solution was kept stirred on a high-speed orbital shaker at 250 rpm for 4 h. Samples of 20 ml were withdrawn from each flask and filtered using filter paper type (CHM, F2042-150) to separate the sorbent. A 10 mL of the filtered solution was pipetted out for analysis to determine the concentration of the remaining contaminant using an atomic absorption spectrophotometer. The number of metal ions sorbed on the solid phase (i.e. iron slag) can be determined by mass balance.

Kinetic studies were investigated with different values of pH (3, 4, 5, 6, and 7), different values of initial concentration (50, 100, 150, 200, and 250 mg/L), different amounts of iron slag dosage (1.0, 3.0, 5.0, 7.0, and 10.0 g) and finally different values of shaking speed (0, 50, 100, 150, 200, and 250 rpm). The results at equilibrium state can be used to calculated the values of contaminant retained on the iron slag phase, q_e, as follows [31]:

$$q_e = \left(C_0 - C_e\right)\frac{V}{m} \tag{7}$$

where C_0 and C_e are the initial and equilibrium concentrations of metal ions in the solution (mg/L), V is the volume of solution in the flask (L), and m is the mass of iron slag added to the flask (g).

The adsorption isotherms are obtained by plotting the weight of the adsorbed solute per unit weight of granular iron slag (q_e) against the equilibrium concentration of the solute in the solution (C_e) [32]. The adsorption efficiency is calculated by the difference in the initial and equilibrium concentrations of pollutant by the following relationship:

$$E_{\text{ad}} = \frac{\left(C_0 - C_e\right)}{C_0} \times 100 \tag{8}$$

4. Results and discussion

4.1. Characterization of iron slag

The chemical composition of iron slag was determined by XRF analysis using an X-ray fluorescence spectrometer (XRF Spectro-Germany). This analysis showed that the main components of the iron slag are oxides of silica (SiO_2), iron (Fe_2O_3), calcium (CaO), aluminum (Al_2O_3) and manganese (MnO) with percentages of 31.21%, 19.95%, 13.48%, 7.93%, and 6.85% respectively. Also, XRD analysis can be used to characterize and identify the mineralogical composition of the used slag based on the crystal structure. In XRD, a sample of slag is placed in a collimated beam of parallel X-rays and diffracted beams with different intensities can be scanned and recorded automatically to draw a plot-related between the intensity of the diffracted beam and two Theta (2θ). Using Rigaku Miniflex 600 XRD analyzer or X-ray diffractometer (40 Kv, 15 mA) with Cu Kα radiation, the records for iron slag with 2θ ranged from 10° to 80° are plotted in Fig. 1 where $FeCaO_2$, CaO, and SiO_2 formed the main crystalline minerals in the used iron slag.

4.2. Equilibrium time and initial pH of the solution

The effect of contact time on the removal of lead ions using 3.0 g granular iron slag added to 100 mL of contaminated solution at 25°C with an initial concentration of 50 mg/L and agitation speed of 250 rpm is plotted in Fig. 2. The removal efficiency was increased dramatically in the initial stages of the contact time and gradually slowed down afterward. The decrease in the rate of the removal efficiency can result from the decrease of the sorption sites; however, the results certified that 90% of lead ions are removed at 120 min and this value was applied for next batch experiments. The same figure illustrates the effect of initial pH with values 3, 4, 5, 6, and 7 on the lead removal efficiencies for contact time not exceeded 180 min. It seems that the best value of initial pH was found to be 4 to achieve the maximum efficiency, however, an increase or decrease in this value can be caused a clear reduction in the removal of metal ions. The formation of protons and precipitates at

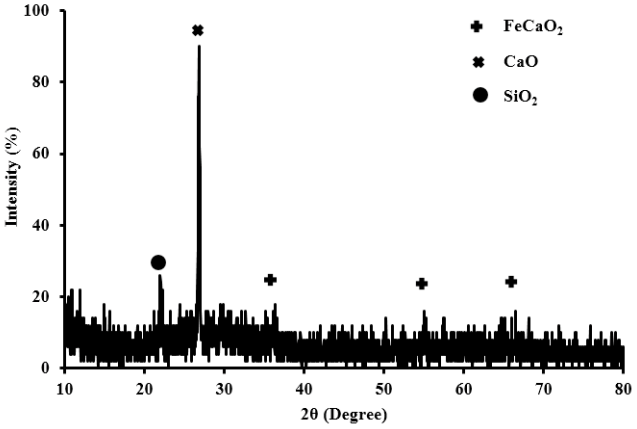

Fig. 1. X-ray diffraction (XRD) analysis for mineralogical characterization of granular iron slag.

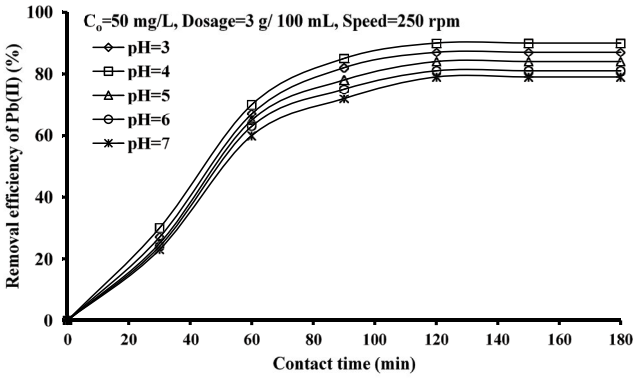

Fig. 2. Removal efficiency of lead ions using granular iron slag at different values of contact time and initial pH.

low and high values of pH respectively may be the major cause for previous behavior [33,34]. Theoretically, the point of zero charge (pH_{pzc}) is the pH at which the sorbent surface charge takes a zero value. At this pH, the charge of the positive surface sites is equal to that of the negative ones. The knowledge of this value allows one to hypothesize on the ionization of functional groups and their interaction with metal species in solution; at solution pHs lower than pH_{pzc}, sorbent surface is positively charged and could interact with metal negative ions while at pHs higher than pH_{pzc}, solid surface is negatively charged and could interact with positive ions. Accordingly, it is expected that the value of pH_{pzc} may be within the range from 3 to 4 and the previous explanation explains why the maximum removal efficiency achieved at a pH value of 4 [35].

4.3. Dosage of iron slag

The dependence of lead ions sorption onto granular iron slag dosage was investigated by changing the quantity of the slag within the range illustrated in Table 1 for batch tests at 25°C; while other conditions, C_0 = 50 mg/L, agitation speed = 250 rpm, and contact time = 120 min with pH value of 4. This table shows that the increase of the sorbent dosage will improve the removal efficiencies and this may be due to the increase of the binding sites. The table certified that the maximum efficiency (=90%) is achieved at a dosage equal to 5.0 g/100 mL and an increase in the quantity of slag does not have a significant effect on the sorption percentage.

4.4. Initial metal concentration

Table 1 elucidates the effect of initial concentration within the range (50–250 mg/L) on the removal efficiency for contact time and sorbent dosage equal to 120 min and 5 g/100 mL respectively. It seems that the increase of the initial concentration up to 200 mg/L will cause a clear decrease in the removal efficiency and there is approximately stabilization in the number of metal ions sorbed on the reactive material after 200 mg/L due to the saturation of the active sites available [36].

4.5. Agitation speed

Removal efficiencies of lead ions by iron slag were measured under the effect of agitation speed which changed from 0 to 250 rpm with the best conditions specified previously. Table 1 shows that about 36% of the metal ions were removed at speed equal to zero and an increase in the speed will increase the uptake of contaminants to reach the removal of 90% at 250 rpm. The increase in the removal efficiency is attributed to the proper contact between the sorbate-sorbent and this will enhance the diffusion of the metal ions from the bulk solution towards the vacant surfaces and, consequently, increase the mass transfer coefficient.

Table 1
Variation of removal efficiencies of lead ions from aqueous solutions onto granular iron slag as a function of dosage, initial concentration, and agitation speed

Operational conditions (pH = 4, t = 120 min)			Removal efficiency (%)
Dosage (g/100 mL)	C_0 (mg/L)	Speed (rpm)	
0.5	50	250	30
1	50	250	60.3
3	50	250	78
5	50	250	90
7	50	250	90.1
10	50	250	90.2
12	50	250	90.4
5	50	250	90
5	100	250	80
5	150	250	64
5	200	250	55
5	250	250	52
5	50	0	36
5	50	50	42
5	50	100	63
5	50	150	80
5	50	200	90
5	50	250	90

4.6. Sorption isotherms

The adsorption isotherms are the essential prerequisites for the design of adsorption systems and they are depended on the equilibrium data. These isotherms are functions correlated between the sorption capacity (q_e) and equilibrium metal concentration in the bulk solution phase (C_e) [37]. The measured sorption data are fitted with non-linear forms of Freundlich and Langmuir models as shown in Fig. 3 where the coefficients of models have been determined using Origin 2018 software. The non-linear analysis was utilized to reduce the percentage of errors in comparison with the linearization of Freundlich and Langmuir isotherms for a description of lead ions sorption onto granular iron slag. The coefficients of the isotherm models and statistical measures such as coefficient of determination (R^2), Chi-square, and sum of squared error (SSE) are mentioned in Table 2. Based on the statistical constants, the Langmuir isotherm model is more representative of a description of the sorption of lead ions onto granular iron slag.

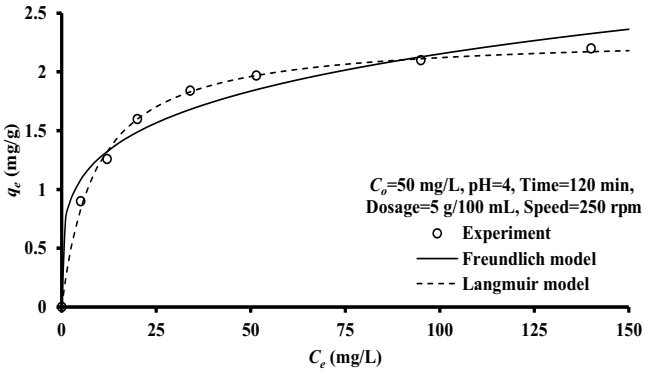

Fig. 3. Concurrence between the experimental results and values predicted by isotherm models for adsorption capacity of lead ions onto granular iron slag.

Table 2
Constants and statistical measures of isotherm models for sorption of lead ions onto granular iron slag

Model	Parameter	Value
Freundlich	K_F (mg/mg)(L/mg)$^{1/n}$	0.7479
	n	4.3570
	R^2	0.9739
	Chi-square (χ^2)	0.0168
	SSE	0.1005
Langmuir	q_{max} (mg/g)	2.309
	b (L/mg)	0.1123
	R^2	0.9974
	Chi-square (χ^2)	0.0017
	SSE	0.0102

The present sorbent has maximum adsorption capacity reached to 2.309 mg/g. The good fit of the data with the Langmuir isotherm indicated that the uniform surfaces of active sites are distributed on the iron slag [38]. This means that the adsorption takes place at specific homogenous sites within the adsorbent and there is no lateral interaction between the sorbed molecules [39]. Further analysis of Langmuir isotherm can be made using the dimensionless equilibrium parameter R_L which is calculated from the division of 1 onto the $(1 + bC_0)$. The value of R_L lies between 0 and 1 for a favorable adsorption, while $R_L > 1$ represents an unfavorable adsorption, for $R_L = 1$ adsorption is linear and if $R_L = 0$, it is irreversible [40]. The dimensionless parameter, R_L is found in the range of 0–1, which confirms the favorable adsorption process for Pb(II) removal.

4.7. Adsorption kinetics

Pseudo-first-order and pseudo-second-order are used to describe the kinetic data measured experimentally to interpret the mechanisms responsible for the sorption process in the interaction between lead ions and iron slag [41]. It is expected that the relationship between the rate constant and metal concentration has a linear trend when the pseudo-first-order applies to the kinetic data [42]. However, if this relationship is not linear, pore diffusion will limit the adsorption process [43]. The kinetics parameters for adsorption of lead ions onto the iron slag are calculated using Origin 2018 software for non-linear regression and listed in Table 3. It seems that the pseudo-second-order is the best-fitting model based on the values of determination coefficient and adsorption capacity (=2.3175 mg/g) which approached from the capacity specified by the equilibrium sorption. The lead uptake of iron slag is attributed to different mechanisms of containing physisorption and chemisorption, ion exchange, as well as surface precipitation. At the

Table 3
Kinetic parameters for the adsorption of lead ions by iron slag

Kinetic model	Parameter	C_0 (mg/L)			
		50	100	150	200
Pseudo-first-order	k_1 (min^{-1})	0.00894	0.00923	0.01578	0.02293
	q_e (mg/g)	1.3942	2.3604	2.4421	2.2536
	R^2	0.9967	0.9988	0.9987	0.9992
Pseudo-second-order	k_2 (g/mg min)	0.00237	0.00157	0.00317	0.00623
	q_e (mg/g)	2.3175	3.8013	3.6159	3.0767
	h (mg/g min)	0.0127	0.0227	0.0414	0.0589
	R^2	0.9959	0.9991	0.9972	0.9965
Intra-particle diffusion	First-portion				
	C	–0.3011	–0.3950	–0.5071	–0.3925
	k_{int} (mg/g min$^{0.5}$)	0.1148	0.1804	0.2586	0.2707
	R^2	0.9883	0.9997	0.9997	0.9997
	Second portion				
	C	–0.1197	–0.0770	0.2142	0.7983
	k_{int} (mg/g min$^{0.5}$)	0.0940	0.1412	0.1702	0.1201
	R^2	0.9893	0.9803	0.9515	0.9271

initial stage, quick adsorption and ion exchange occurred; then, the hydrolysis of slag and precipitation kinetics took place [44].

The intra-particle diffusion model (Fig. 4) indicated that there is more than one mechanism governed the sorption process and intra-particle diffusion was not the rate-limiting step. This means that the external mass transfer was predominant in the early stages and, then, intra-particle diffusion can be controlled as plotted in the second linear portion [45,46]. The higher slopes of the first lines (k_{int} ranged from 0.1148 to 0.2707) certifies that the rate of removal is greater in the initial stages in comparison with values of slopes for the second line (k_{int} ranged from 0.0940 to 0.1702). The decrease in the rate of removal may result from the reduction of the concentration gradient. Finally, Table 4 presents a comparison between the value of adsorption capacity of lead ions onto the iron slag achieved in the present study and that values for the same contaminant on the different sorbents mentioned in the previous studies [47–52]. In spite of this adsorption capacity is less than that achieved in these studies but the value of hydraulic conductivity for iron slag (2.69×10^{-3} m/s) can be considered very suitable for PRB technology.

4.8. Fourier transform infrared analysis

The infrared spectrum of slag is plotted in Fig. 5 and this figure reveals that the presence of absorption bands corresponding to the Fe–O and Ca–O vibrations at 700 and 450 cm^{-1}, respectively. The presence of calcium could be associated with carbonates species (stretching bands near 1,435 cm^{-1}) which are apparently related to the existence of calcite and this is in agreement with the results of the XRF test. Stretching vibrations of the surface hydroxyl groups (Fe–OH) are found at 3,695 cm^{-1} and vibration at 1,635 cm^{-1} can be attributed to the bending of adsorbed water between the layers. Due to the presence of Fe in the composition of the slag, the experimental results proved that the iron oxide surface sites are the predominant in the removal of lead ions from aqueous solutions. The calcium occupies these sites and when calcium oxide dissolved in the aqueous solution both the hydrolysis and ion exchange processes begin. Under acidic best condition (i.e. pH of 4), the calcium is changed by the hydrogen and lead ions according to the following reactions:

$$\left(Fe-O^{-}\right)_2 Ca^{+2} + H_3O \rightarrow 2\left(Fe-OH\right) + Ca^{+2} + OH \quad (9)$$

$$\left(Fe-O^{-}\right)_2 Ca^{+2} + 2Pb^{+2} \rightarrow 2Fe-OPb + Ca^{+2} \quad (10)$$

The reactions probably occur before saturation when the lead ions are completely removed with an increase of final pH values to reach 6.4. Accordingly, the removal process depends primarily on the release of calcium ions within the slag and they replaced by lead ions.

4.9. Scanning electron microscopy and energy-dispersive X-ray spectroscopy analysis

Microstructure of iron slag was represented by the scanning electron microscopy (SEM) where an electron beam can be directed to the sample and measurement of the scattered electrons. The tests of the SEM can provide a detailed analysis of the shape, size, and texture of the iron slag before and after the sorption of lead ions. In addition, this test in conjugation with energy-dispersive X-ray spectroscopy (EDS) can specify all elements available in the sample and this will be very fruitful in the identification of the

Table 4
Maximum adsorption capacities for iron slag in comparison with different reactive materials adopted from previous studies for removal of lead ions from aqueous solutions

Material	q_{max} (mg/g)	References
Iran slag	2.309	Present study
Ti(IV) iodovanadate cation exchanger	18.8	[47]
Bituminous coal	8.89	[48]
Bentonite	15.38	[49]
Carbon nanotubes	12.41	[50]
Carbon aerogel	34.72	[51]
Eichhornia carbon	16.61	[52]

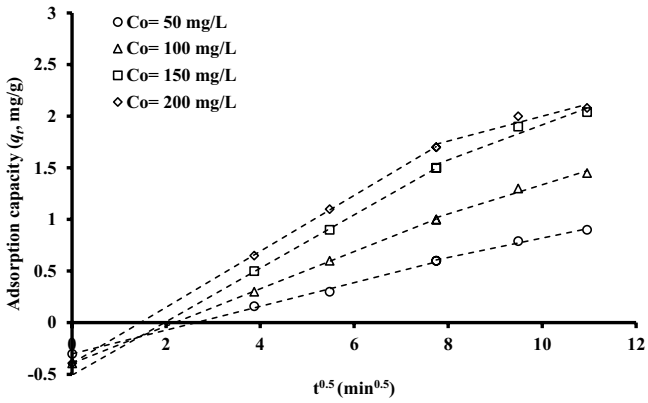

Fig. 4. Intra-particle diffusion model for sorption of lead ions from aqueous solution onto granular iron slag.

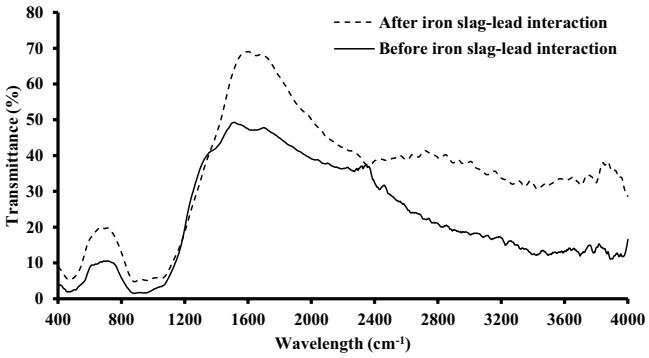

Fig. 5. FTIR spectra of iron slag before and after interaction with aqueous solution contaminated with lead.

characteristics of the used sorbent. It is that the pores were filled up and the surface was less rough after adsorption in comparison with original slag. This is because the active sites inside the slag pores are loaded with the contaminant, in addition to the dissolution of CaO, which formed lead hydroxide and caused the filling gaps and forming crystals on the surface.

The EDS analysis (Fig. 6) explains the elements constituted of the granular iron slag after adsorption of lead ions. This figure elucidates that there is flocculation in the particles and the mixture has more strength due to the clear reduction in the air voids and bonding of particles. Also, the calcium hydroxide in the slag sample is dissolved after the adsorption process and this can be caused by the change in the surface morphology as plotted in Fig. 6.

4.10. Lead ions transport in the subsurface environment

The advection-dispersion equation describes the transport of lead ions through the porous medium such as PRB undergoing equilibrium sorption and this equation can be written as:

$$D_z \frac{\partial^2 C}{\partial z^2} - V_z \frac{\partial C}{\partial z} + \frac{\rho b}{n_B} \frac{\partial q_e}{\partial t} = \frac{\partial C}{\partial t} \tag{11}$$

where C is the lead ions concentration in the aqueous solution, q_e is the adsorption capacity, t is the travel time, D is the hydrodynamic dispersion coefficient, V is the mean pore velocity, and z is the travel distance.

The third term in the left-hand side of Eq. (11) represents the reaction (i.e. sorption) process and it can be governed by Langmuir isotherm as proved by the batch study described previously. Hence, the batch results play a significant role in the description of the transformation process of the reactive contaminant within the advection-dispersion equation. By substituting the Langmuir model into Eq. (11), the retardation factor (R) can be represented as follows:

$$D_z \frac{\partial^2 C}{\partial z^2} - V_z \frac{\partial C}{\partial z} + \frac{\rho b}{n_B} \frac{\partial q_e}{\partial t} = R \frac{\partial C}{\partial t} \tag{12}$$

$$R = 1 + \frac{\rho d}{n} \left(\frac{q_{\max} b}{\left(1 + b C_e\right)^2} \right) \tag{13}$$

where ρ_d is the bulk density of the sorbent (i.e. iron slag, g/cm^3) and n is the porosity of the sorbent.

The retardation factor reflects the ability of the PRB to retard the migration of the contaminant and the high value of R will increase the longevity of the barrier to satisfy the environmental regulations for the concentration of a contaminant at its down gradient. Using the values of Langmuir constants listed in Table 2 in combination with ρ_d of 2.0264 and n of 0.41, the values of R can be calculated from Eq. (13) as plotted in Fig. 7. It seems that the values of the retardation factor (i.e. functionality of the barrier) reduce from 1.28×10^6 to 4,582 with an increase of the equilibrium concentration for metal ions from 0 to 140 mg/L respectively.

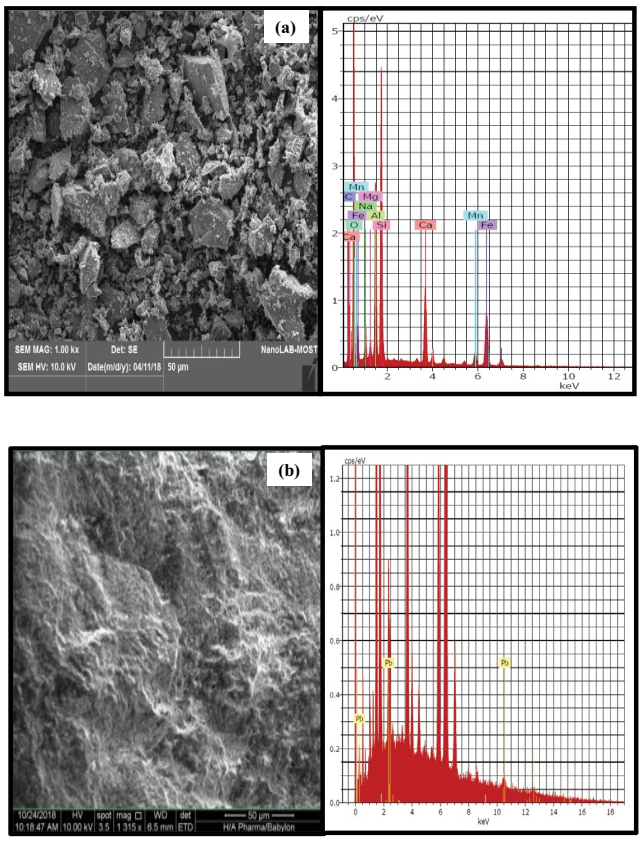

Fig. 6. SEM/EDS for iron slag (a) before and (b) after the sorption of lead ions from aqueous solution.

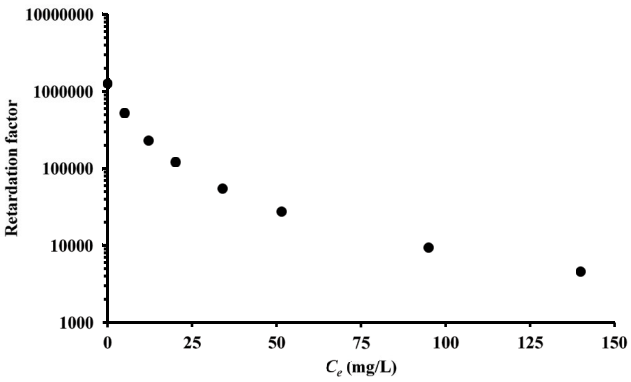

Fig. 7. Retardation factor as a function of equilibrium concentration based on Langmuir sorption isotherm for lead migration through iron slag bed.

5. Conclusion

The interaction of iron slag – aqueous solution contaminated with lead ions was studied in the batch tests and results proved the ability of this by-product material in the elimination of the pollution. Results signified that the best conditions for this interaction were pH of 4, the contact time of 120 min, sorbent dosage of 5 g/100 mL, and agitation speed of 250 rpm to achieve the maximum removal efficiency of 90% and adsorption capacity of 2.309 mg/g. Based

on the coefficient of determination, the Langmuir isotherm model can be described in a well manner the sorption data and pseudo-second-order has a good ability in the representation of kinetic measurements. Characterization of iron slag by XRF, XRD, Fourier transform infrared (FTIR), SEM and EDS tests signified that the iron oxide surface sites are the predominant in the removal of lead ions due to dissolve of calcium oxide and this will enhance both the hydrolysis and ion exchange. The outputs of the present study revealed that the iron slag can be used in the future as a reactive material in the PRB technology especially the theoretical estimation for retardation factor in the continuous transport reached a high value (=500,000) for equilibrium concentration of 5 mg/L.

Acknowledgment

The author would like to gratefully acknowledge the technical support of the Environmental Engineering Department/University of Baghdad during this work.

References

[1] F.R. Evanko, D.A. Dzombak, Remediation of Metals Contaminated Soils and Groundwater, Groundwater Remediation Technologies Analysis Centre, Pittsburg, Pa, USA, Tech. Rep. TE-97-01, 1997.
[2] D.W. Blowes, C.J. Ptacek, S.G. Benner, C.W.T. McRae, T.A. Bennett, R.W. Puls, Treatment of inorganic contaminants using permeable reactive barriers, J. Contam. Hydrol., 45 (2000) 123–137.
[3] M.A. Carey, B.A. Fretwell, N.G. Mosley, J.W.N. Smith, Guidance on the Use of Permeable Reactive Barriers for Remediating Contaminated Groundwater, National Groundwater and Contaminated Land Centre, UK Environment Agency, Bristol, Report NC/01/51, 2002.
[4] K. Komnitsas, G. Bartzas, K. Fytas, I. Paspaliaris, Long-term efficiency and kinetic evaluation of ZVI barriers during clean-up of copper containing solutions, Miner. Eng., 20 (2007) 1200–1209.
[5] F. Obiri-Nyarko, S.J. Grajales-Mesa, G. Malina, An overview of permeable reactive barriers for *in situ* sustainable groundwater remediation, Chemosphere, 111 (2014) 243–259.
[6] V.K. Gupta, Equilibrium uptake, sorption dynamics, process development, and column operations for the removal of copper and nickel from aqueous solution and wastewater using activated slag, a low-cost adsorbent, Ind. Eng. Chem. Res., 37 (1998) 192–202.
[7] L. Curković, Š. Cerjan-Stefanović, A. Rastovèan-Mioè, Batch Pb^{2+} and Cu^{2+} removal by electric furnace slag, Water Res., 35 (2000) 3436–3440.
[8] A.A.H. Faisal, Z.A. Hmood, Groundwater protection from cadmium contamination by zeolite permeable reactive barrier, Desal. Wat. Treat., 53 (2015) 1377–1386.
[9] A.A.H. Faisal, M.D. Ahmed, Remediation of groundwater contaminated with copper ions by waste foundry sand permeable barrier, J. Eng., 20 (2014) 62–77.
[10] A.A.H. Faisal, L.A. Naji, Simulation of ammonia nitrogen removal from simulated wastewater by sorption onto waste foundry sand using artificial neural network, Assoc. Arab Univ. J. Eng. Sci., 26 (2019) 28–34.
[11] A.H. Sulaymon, A.A.H. Faisal, Q.M. Khaliefa, Cement kiln dust (CKD)-filter sand permeable reactive barrier for the removal of Cu(II) and Zn(II) from simulated acidic groundwater, J. Hazard. Mater., 297 (2015) 160–172.
[12] A.H. Sulaymon, A.A.H. Faisal, Z.T. Abd Ali, Performance of granular dead anaerobic sludge as permeable reactive barrier for containment of lead from contaminated groundwater, Desal. Wat. Treat., 56 (2015) 327–337.
[13] A.A.H. Faisal, Z.T. Abd Ali, Groundwater protection from lead contamination using granular dead anaerobic sludge biosorbent as permeable reactive barrier, Desal. Wat. Treat., 57 (2016) 3891–3903.
[14] A.A.H. Faisal, T.R. Abbas, S.H. Jassam, Removal of zinc from contaminated groundwater by zero-valent iron permeable reactive barrier, Desal. Wat. Treat., 55 (2015) 1586–1597.
[15] H.M. Rashid, A.A.H. Faisal, Removal of dissolved trivalent chromium ions from contaminated wastewater using locally available raw scrap iron-aluminum waste, Al-Khwarizmi Eng. J., 15 (2019) 134–143.
[16] A.A.H. Faisal, Effect of pH on the performance of olive pips reactive barrier through the migration of copper-contaminated groundwater, Desal. Wat. Treat., 57 (2016) 4935–4943.
[17] V.K. Jha, Y. Kameshima, A. Nakajima, K. Okada, Hazardous ions uptake behavior of thermally activated steel-making slag, J. Hazard. Mater., B114 (2004) 139–144.
[18] J. Bijen, Benefits of slag and fly ash, Constr. Build. Mater., 10 (1996) 309–314.
[19] M. Penpolcharoen, Utilization of secondary lead slag as construction material, Cem. Concr. Res., 35 (2005) 1050–1055.
[20] W. Cha, J. Kim, H. Choi, Evaluation of steel slag for organic and inorganic removals in soil aquifer treatment, Water Res., 40 (2006) 1034–1042.
[21] S.V. Dimitrova, D.R. Mehandgiev, Lead removal from aqueous solutions by granulated blast-furnace slag, Water Res., 32 (1998) 3289–3292.
[22] N. Ortiz, M.A.F. Pires, J.C. Bressiani, Use of steel converter slag as nickel adsorber to wastewater treatment, Waste Manage., 21 (2001) 631–635.
[23] D.-H. Kim, M.-C. Shin, H.-D. Choi, C.-I. Seo, K. Baek, Removal mechanisms of copper using steel-making slag: adsorption and precipitation, Desalination, 223 (2008) 283–289.
[24] N.M. Reza, O. Sasan, Absorption of lead ions by various types of steel slag iron, J. Chem. Chem. Eng., 27 (2008) 69–75.
[25] H. Zheng, D. Liu, Y. Zheng, S. Liang, Z. Liu, Sorption isotherm and kinetic modeling of aniline on Cr-bentonite, J. Hazard. Mater., 167 (2009) 141–147.
[26] K. Foo, B. Hameed, Insights into the modeling of adsorption isotherm systems, Chem. Eng. J., 156 (2010) 2–10.
[27] H.K. Hansen, F. Arancibia, C. Gutiérrez, Adsorption of copper onto agriculture waste materials, J. Hazard. Mater., 180 (2010) 442–448.
[28] P.R. Puranik, J.M. Modak, K.M. Paknikar, A comparative study of the mass transfer kinetics of metal biosorption by microbial biomass, Hydrometallurgy, 52 (1999) 189–197.
[29] Y.S. Ho, G. McKay, Pseudo-second order model for sorption processes, Process Biochem., 34 (1999) 451–465.
[30] M. Arshadi, M.J. Amiri, S. Mousavi, Kinetic, equilibrium and thermodynamic investigations of Ni(II), Cd(II), Cu(II) and Co(II) adsorption on barely straw ash, Water Resour. Ind., 6 (2014), 1–17.
[31] L.K. Wang, J.-H. Tay, S.T.L. Tay, Y.-T. Hung, Environmental Bioengineering, Part of the Handbook of Environmental Engineering Book Series, Vol. 11, Springer, ISBN 978-1-58829-493-7, 2010.
[32] J.C. Crittenden, T.F. Speth, D.W. Hand, P.J. Luft, B. Lykins, Evaluating multicomponent competitive adsorption in fixed beds, J. Environ. Eng., 113 (1987) 1363–1375.
[33] S.U. Kurnaz, H. Buyukgungor, Assessment of various biomasses in the removal of phenol from aqueous solutions, J. Microbiol. Biochem. Technol., 1 (2009) 47–50.
[34] A.H. Sulaymon, A.A. Mohammed, T.J. Al-Musawi, Competitive biosorption of lead, cadmium, copper, and arsenic ions using algae, Environ. Sci. Pollut. Res., 20 (2013) 3011–3023.
[35] K.A. Krishnan, T.S. Anirudhan, Removal of mercury(II) from aqueous solutions and chlor-alkali industry effluent by steam activated and sulphurised activated carbons prepared from bagasse pith: kinetics and equilibrium studies, J. Hazard. Mater., 92 (2002) 161–183.
[36] R. Qadeer, A.H. Rehan, A study of the adsorption of phenol by activated carbon from aqueous solutions, Turk. J. Chem., 26 (2002) 357–362.

[37] O. Hamdaoui, E. Naffrechoux, Modeling of adsorption isotherms of phenol and chlorophenols onto granular activated carbon: part I. Two-parameter models and equations allowing determination of thermodynamic parameters, J. Hazard. Mater., 147 (2007) 381–394.
[38] Y. Bulut, H. Aydın, A kinetics and thermodynamics study of methylene blue adsorption on wheat shells, Desalination, 194 (2006) 259–267.
[39] N. Benderdouche, B. Bestani, M. Hamzaoui, The use of linear and nonlinear methods for adsorption isotherm optimization of basic green 4-dye onto sawdust-based activated carbon, J. Mar. Environ. Sci., 9 (2018) 1110–1118.
[40] M.K. Rai, G. Shahi, V. Meena, R. Meena, S. Chakraborty, R.S. Singh, B.N. Rai, Removal of hexavalent chromium Cr(VI) using activated carbon prepared from mango kernel activated with H_3PO_4, Resour.-Effic. Technol., 2 (2016) S63–S70.
[41] Y.S. Ho, G. McKay, The kinetics of sorption of divalent metal ions onto sphagnum moss peat, Water Res., 34 (2000) 735–742.
[42] E.M. Kalhori, T.J. Al-Musawi, E. Ghahramani, H. Kazemian, M. Zarrabi, Enhancement of the adsorption capacity of the light-weight expanded clay aggregate surface for the metronidazole antibiotic by coating with MgO nanoparticles: studies on the kinetic, isotherm, and effects of environmental parameters, Chemosphere, 175 (2017) 8–20.
[43] M.N. Sepehr, A. Amrane, K.A. Karimaian, M. Zarrabi, H.R. Ghaffari, Potential of waste pumice and surface modified pumice for hexavalent chromium removal: characterization, equilibrium, thermodynamic and kinetic study, J. Taiwan Inst. Chem. Eng., 45 (2014) 635–647.
[44] X. Chen, W.H. Hou, G.L. Song, Q.H. Wang, Adsorption of Cu, Cd, Zn and Pb ions from aqueous solutions by electric arc furnace slag and the effects of pH and grain size, Chem. Biochem. Eng. Q., 25 (2011) 105–114.
[45] M.H. Kalavathy, T. Karthikeyan, S. Rajgopal, L.R. Miranda, Kinetic and isotherm studies of Cu(II) adsorption onto H_3PO_4-activated rubber wood sawdust, J. Colloid Interface Sci., 292 (2005) 354–362.
[46] I. Tan, A. Ahmad, B. Hameed, Adsorption isotherms, kinetics, thermodynamics and desorption studies of 2, 4, 6-trichlorophenol on oil palm empty fruit bunch-based activated carbon, J. Hazard. Mater., 164 (2009) 473–482.
[47] M. Naushad, Z.A. ALOthman, R. Awual, M.M. Alam, G.E. Eldesoky, Adsorption kinetics, isotherms, and thermodynamic studies for the adsorption of Pb^{2+} and Hg^{2+} metal ions from aqueous medium using Ti(IV) iodovanadate cation exchanger, Ionics, 21 (2015) 2237–2245.
[48] D. Singh, N.S. Rawat, Sorption of Pb(II) by bituminous coal, Ind. J. Chem. Technol., 4 (1995) 49–50.
[49] G. Bereket, A.Z. Aroguz, M.Z. Ozel, Removal of Pb(II), Cd(II), Cu(II) and Zn(II) from aqueous solutions by adsorption of bentonite, J. Colloid Interface Sci., 183 (1997) 338–343.
[50] Y.H. Li, Z. Di, J. Ding, D. Wu, Z. Luan, Y. Zhu, Adsorption thermodynamic, kinetic and desorption studies of Pb^{2+} on carbon nanotubes, Water Res., 39 (2005) 605–609.
[51] J. Goel, K. Kadirvelu, C. Rajagopal, V.K. Garg, Removal of lead(II) from aqueous solution by adsorption on carbon aerogel using a response surface methodological approach, Ind. Eng. Chem. Res., 44 (2005) 1987–1994.
[52] P. Shekinath, K. Kadirvelu, P. Kanmani, P. Senthilkumar, V. Subburam, Adsorption of lead(II) from aqueous solution by activated carbon prepared from *Eichhornia*, J. Chem. Technol. Biotechnol., 77 (2002) 1–7.